



3 4456 0321904 1

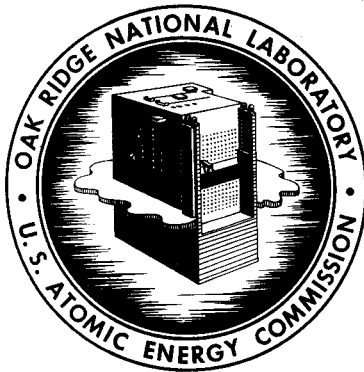
OAK RIDGE NATIONAL LIBRARY
DOCUMENT COLLECTION

1

ORNL-4052
UC-25 - Metals, Ceramics, and Materials

CHARACTERIZATION AND PRODUCTION OF
 U_3O_8 FOR THE HIGH FLUX ISOTOPE REACTOR

W. J. Werner
J. R. Barkman



OAK RIDGE NATIONAL LABORATORY

operated by

UNION CARBIDE CORPORATION

for the

U.S. ATOMIC ENERGY COMMISSION

Printed in the United States of America. Available from Clearinghouse for Federal
Scientific and Technical Information, National Bureau of Standards,
U.S. Department of Commerce, Springfield, Virginia 22151
Price: Printed Copy \$3.00; Microfiche \$0.65

LEGAL NOTICE

This report was prepared as an account of Government sponsored work. Neither the United States, nor the Commission, nor any person acting on behalf of the Commission:

- A. Makes any warranty or representation, expressed or implied, with respect to the accuracy, completeness, or usefulness of the information contained in this report, or that the use of any information, apparatus, method, or process disclosed in this report may not infringe privately owned rights; or
- B. Assumes any liabilities with respect to the use of, or for damages resulting from the use of any information, apparatus, method, or process disclosed in this report.

As used in the above, "person acting on behalf of the Commission" includes any employee or contractor of the Commission, or employee of such contractor, to the extent that such employee or contractor of the Commission, or employee of such contractor prepares, disseminates, or provides access to, any information pursuant to his employment or contract with the Commission, or his employment with such contractor.

ORNL-4052

Contract No. W-7405-eng-26

METALS AND CERAMICS DIVISION

CHARACTERIZATION AND PRODUCTION OF U_3O_8 FOR THE
HIGH FLUX ISOTOPE REACTOR

W. J. Werner J. R. Barkman

APRIL 1967

OAK RIDGE NATIONAL LABORATORY
Oak Ridge, Tennessee
operated by
UNION CARBIDE CORPORATION
for the
U.S. ATOMIC ENERGY COMMISSION

MARTIN MARIETTA ENERGY SYSTEMS LIBRARIES

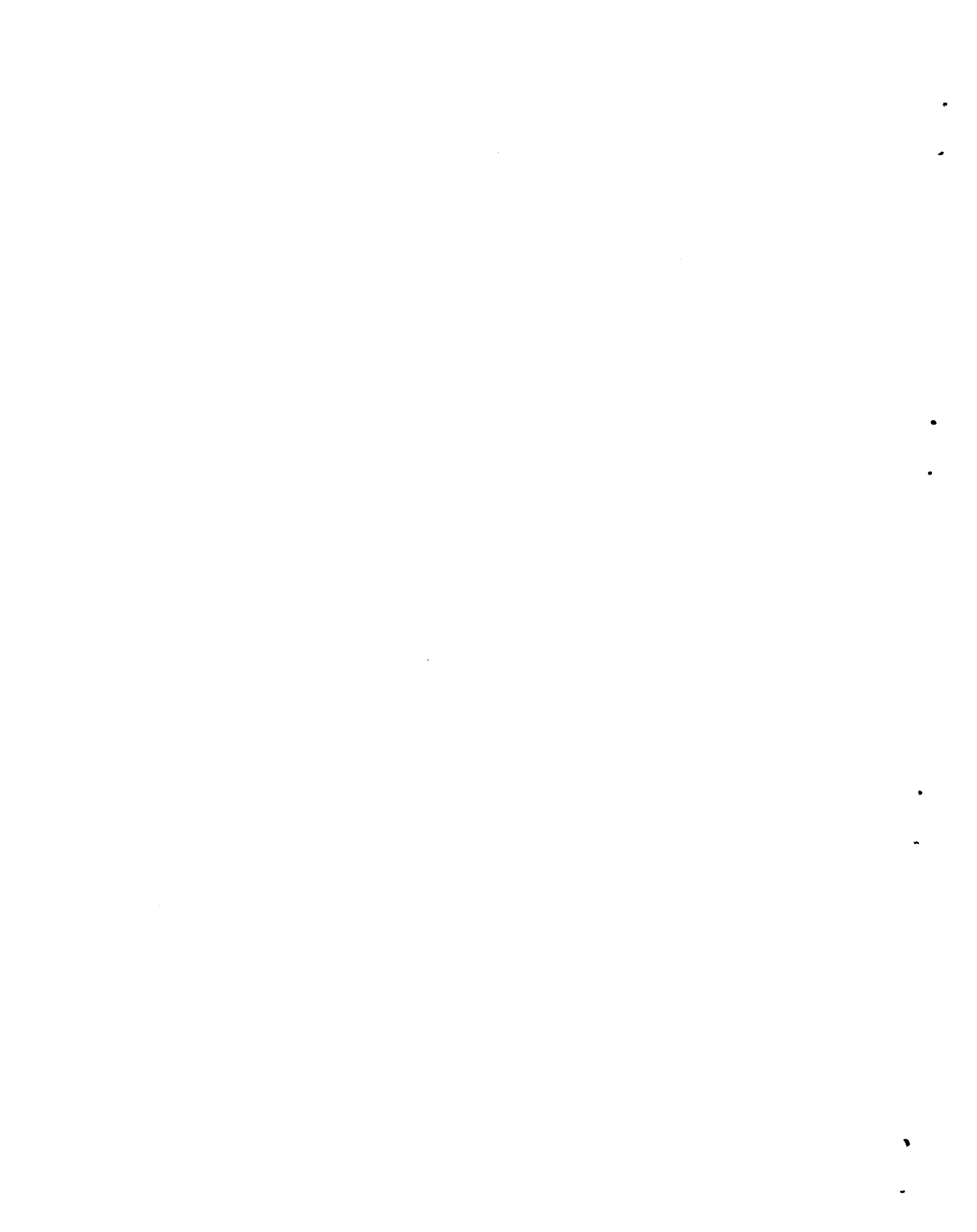


3 4456 0321904 1



CONTENTS

	<u>Page</u>
Abstract	1
Introduction	1
Reactor Description	4
Oxide Specification	5
Preparation of U_3O_8	6
Conversion of Metal to U_3O_8 and Dissolution	8
Precipitation	8
Calcining and Presizing	9
Sintering and Final Sizing	10
Sampling and Cross Blending	10
Investigation of Different Grades of Oxide	12
Experimental Investigations	12
Oxide Microstructure	13
Comminution During Plate Fabrication	13
X-Ray Studies	17
Differential Thermal and Thermogravimetric Analyses	21
Chemical and Surface Area Analysis	22
X-Ray Attenuation Differences	25
Conclusions	27
Acknowledgments	28
Appendix: Analytical Data on the Individual Batches of U_3O_8	29



CHARACTERIZATION AND PRODUCTION OF U₃O₈ FOR THE
HIGH FLUX ISOTOPE REACTOR

W. J. Werner J. R. Barkman¹

ABSTRACT

The preparation and characterization of U₃O₈ used in the Oak Ridge National Laboratory HFIR fuel plates are described. The high performance required for the fuel plates demands uniformity of fuel distribution, and so nondestructive techniques were developed to detect and evaluate changes in fuel loading. Commercial oxide suffered severe comminution during plate fabrication and thereby biased plate homogeneity inspection. This factor plus the absence of irradiation data on this differing material under HFIR burnup made the use of such an oxide questionable. Morphology, microstructure, and behavior in plate fabrication are compared for a commercial oxide and an oxide manufactured at Y-12. The Y-12 oxide manufacturing process consists of peroxide precipitation from uranyl nitrate solution, calcining, and sintering. The propensity toward comminution during fabrication shown by commercial U₃O₈ is reflected by a surface area greater than 0.05 m²/g, as measured by a static BET krypton-adsorption method. Consistent with this, the commercial U₃O₈ particles exhibited a large number of microcracks when observed under the microscope, while the Y-12 oxide particles were rounded and contained few cracks.

INTRODUCTION

Aluminum-base dispersions of U₃O₈ were chosen for the fuel of the Oak Ridge National Laboratory High Flux Isotope Reactor on the basis of previous extensive studies at ORNL. Initial fuel-plate development for the HFIR utilized a silicon-stabilized boronated uranium-aluminum alloy fuel. However, segregation of uranium and boron in these alloys² negated their use, since a high degree of control is required of fuel loading and distribution in each plate. Unlike UO₂ and UC, U₃O₈ does not react with

¹Uranium Chemistry Group, Y-12 Plant.

²D. T. Bourgette, W. J. Kucera, J. H. Erwin, and T. D. Watts, Metallurgy Div. Ann. Progr. Rept. May 31, 1961, ORNL-3160, pp. 101-103.

the aluminum matrix during fuel element processing³⁻⁵ requiring temperatures as high as 600°C. These dispersions exhibit better corrosion resistance in water at 180°F than do UC₂-aluminum dispersions or an Al-48% U-3% Si alloy.⁶ Additionally, the compound U₃O₈ can be produced economically and has a relatively high uranium content. The irradiation performance of U₃O₈-aluminum dispersions at HFIR burnup conditions was not fully evaluated prior to the initiation of fuel-plate production. Previous ORNL studies⁷ at pool-type reactor temperatures had shown that these dispersions were relatively insensitive to radiation damage, as manifested by the absence of blistering and negligible volume changes during burnups as high as 7.7×10^{20} fissions/cm³. Void formation and core separation causing blisters have been observed⁸ in similar samples irradiated to 1.1×10^{21} fissions/cm³ in a special ETR loop at temperatures considerably in excess of those expected in HFIR but whose actual values were not known. Subsequently, satisfactory performance was demonstrated^{9,10} by irradiation in the same facility, but with proper temperature control, to 1.6×10^{21} fissions/cm³ at HFIR temperatures.

³R. C. Waugh, The Reaction and Growth of Uranium Dioxide-Aluminum Fuel Plates and Compacts, ORNL-2701 (March 9, 1959).

⁴W. C. Thurber and R. J. Beaver, Dispersions of Uranium Carbides in Aluminum Plate-Type Research Reactor Fuel Elements, ORNL-2618 (Nov. 5, 1959).

⁵Metals Handbook, 8th ed., Vol. 1, pp. 931-36, ASM, Novelty, Ohio (1961).

⁶W. J. Kucera, Metallurgy Div. Ann. Progr. Rept. Sept. 1, 1959, ORNL-2839, pp. 262-65.

⁷A. E. Richt, C. F. Leitten, Jr., and R. J. Beaver, "Radiation Performance and Induced Transformations in Aluminum-Base Fuels," pp. 469-88 in Research Reactor Fuel Element Conference, September 17-19, 1962, Gatlinburg, Tennessee, TID-7642, Book 2 (1963).

⁸M. J. Graber et al., Results of ATR Sample Fuel Plate Irradiation Experiment, IDO-16958 (March 23, 1964).

⁹A. E. Richt and M. M. Martin, "Irradiation Testing of Aluminum-Base Miniature Fuel Plates," Metals and Ceramics Div. Ann. Progr. Rept. June 30, 1966, pp. 109-11.

¹⁰V. A. Walker, M. J. Graber, and G. W. Gibson, ATR Fuel Materials Development Irradiation Results, Part II, IDO-17157 (June 1966).

The chief disadvantages of low thermal conductivity and brittleness, which are characteristic of U_3O_8 , are lessened by dispersing the compound in aluminum. During fuel-plate development, a dense inert grade of U_3O_8 with an oxygen-to-uranium ratio near stoichiometric was used. This fissile material was free of agglomerates, platelets, rods, and clinging surface fines, which give rise to fragmentation and stringering during processing. Additionally, the particle-size range was closely controlled to minimize fission-fragment damage to the matrix aluminum and to provide good dispersion characteristics. A "dead burned" U_3O_8 developed at the Oak Ridge Y-12 Plant of the Union Carbide Nuclear Company met these requirements for the fuel-plate development program.

Upon completion of the ORNL development work, a contract was negotiated with a commercial fuel element manufacturer for the production of a number of reactor core loadings. Under the terms of the contract the manufacturer was to procure commercial oxide for these elements according to a set of specifications that were a direct result of the HFIR fuel-plate development program. Twice contracts were negotiated with commercial suppliers, but both vendors failed to produce oxide meeting the HFIR specifications and showed no interest in making the necessary changes in their production procedures. To enable the fuel-element fabricator to meet the HFIR schedule, the U_3O_8 was obtained from the Y-12 plant of the Union Carbide Nuclear Company. The commercial oxide consisted of badly cracked irregular particles, which stringered during roll bonding, resulting in a very fine oxide particle. While experimental information was not available on such oxides, indications were that they would have inferior radiation resistance properties. Neither time nor money was available for such testing. Since this area was one of the major questions in the reactor operation, a strong incentive existed to use the proven Y-12-type oxide, which meets the specifications. Since these oxides all fabricated differently, they required different size dies and tools. Therefore it was desirable to adopt one type for the entire production.

This report sets forth the method used by Y-12 for producing over 300 kg of HFIR-grade oxide for the fuel element manufacturer and elucidates the differences between plates produced from different grades of oxide.

REACTOR DESCRIPTION

The HFIR, designed and built for the synthesis of transplutonium elements, operates at an unperturbed thermal neutron flux of about 5.5×10^{15} neutrons $\text{cm}^{-2} \text{sec}^{-1}$. The distinguishing characteristic of the system is the tremendous amount of power generated (100 Mw) in the small reactor core containing the compact (17 in. in diameter \times 20 in. high) and high-performance fuel assembly. Design of the fuel assembly and fuel plate is schematically illustrated in Fig. 1. The fuel plates are unique in that they contain a specified variable fuel load across the plate.¹¹ This design feature was necessary to minimize radial power peaking and to permit operation at a higher total power level. Powder-metallurgy dispersion plate-fabrication techniques were found to be

¹¹R. D. Cheverton, "Nuclear Design of the HFIR," pp. 89-98 in Research Reactor Fuel Element Conference, September 17-19, 1962, Gatlinburg, Tennessee, TID-7642, Book 1 (1963).

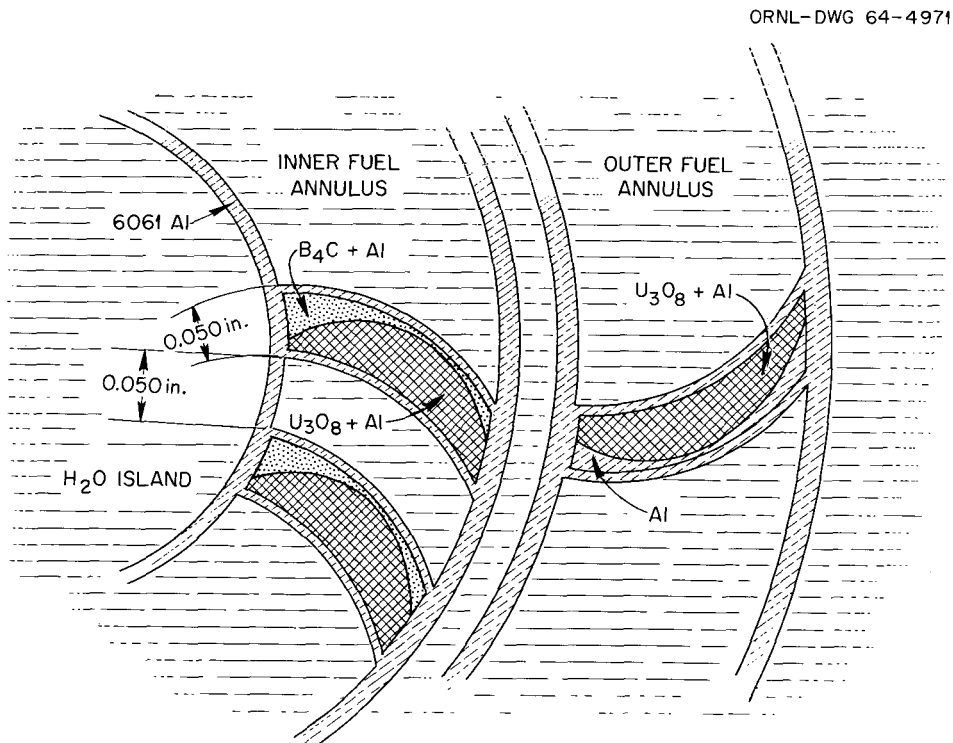


Fig. 1. Schematic Illustration of Fuel Element and Fuel Plate Design.

consistent with the concomitant required degree of control of fuel loading and distribution.¹²

To ensure reliable fuel element performance, specifications on uranium homogeneity in HFIR fuel plates far exceed any other known specification. Briefly, it is required that no spot 5/64 in. in diameter within the fueled area of a plate exceed its theoretical fuel loading by more than 27%. Additionally, the average fuel loading within any 5/64-in.-wide section parallel to the core and varying in length from approximately 1/2 to 1 1/2 in. cannot deviate from the specified loading by more than 12%. This length depends upon the uranium concentration preceding any change in concentration and the magnitude of that change. This difficult specification is complicated by the variable fuel loading of the plates. An x-ray attenuation method was developed for measuring fuel concentration variation within each fuel plate.¹³

OXIDE SPECIFICATION¹⁴

The following oxide specification was established for use with the first commercial contract for producing HFIR fuel elements by measurement of the properties of development-grade oxide produced by the process developed by the Y-12 Uranium Chemistry Group.

1. The U_3O_8 used as the fuel shall be a high-fired or dead-burned oxide having a density greater than 8.2 g/cm³, as determined by a toluene pycnometer, and a surface area of less than 0.05 m²/g, as determined by a static krypton BET determination.¹⁵

¹²W. J. Werner, T. D. Watts, and J. P. Hammond, Metals and Ceramics Div. Ann. Progr. Rept. May 31, 1963, ORNL-3470, pp. 173-74.

¹³B. E. Foster, S. D. Snyder, and R. W. McClung, Continuous Scanning X-Ray Attenuation Technique for Determining Fuel Inhomogeneities in Dispersion Core Fuel Plates, ORNL-3737 (January 1965).

¹⁴G. M. Adamson, Jr., and J. R. McWherter, Specifications for High Flux Isotope Reactor Fuel Elements HFIR-FE-1, ORNL-TM-902 (August 1964).

¹⁵J. L. Botts, "Surface Area of Solids, Krypton Adsorption Method," Method Nos. 1 105 and 9 00605 (12-28-61) ORNL Master Analytical Manual, TID-7015, Supplement 5 (September 1963).

2. The total uranium concentration shall exceed 84.5 wt % with a maximum UO_2 content of 1.0%.

3. An analysis shall be required for each batch of U_3O_8 . The impurities in the U_3O_8 shall not exceed the limits specified below:

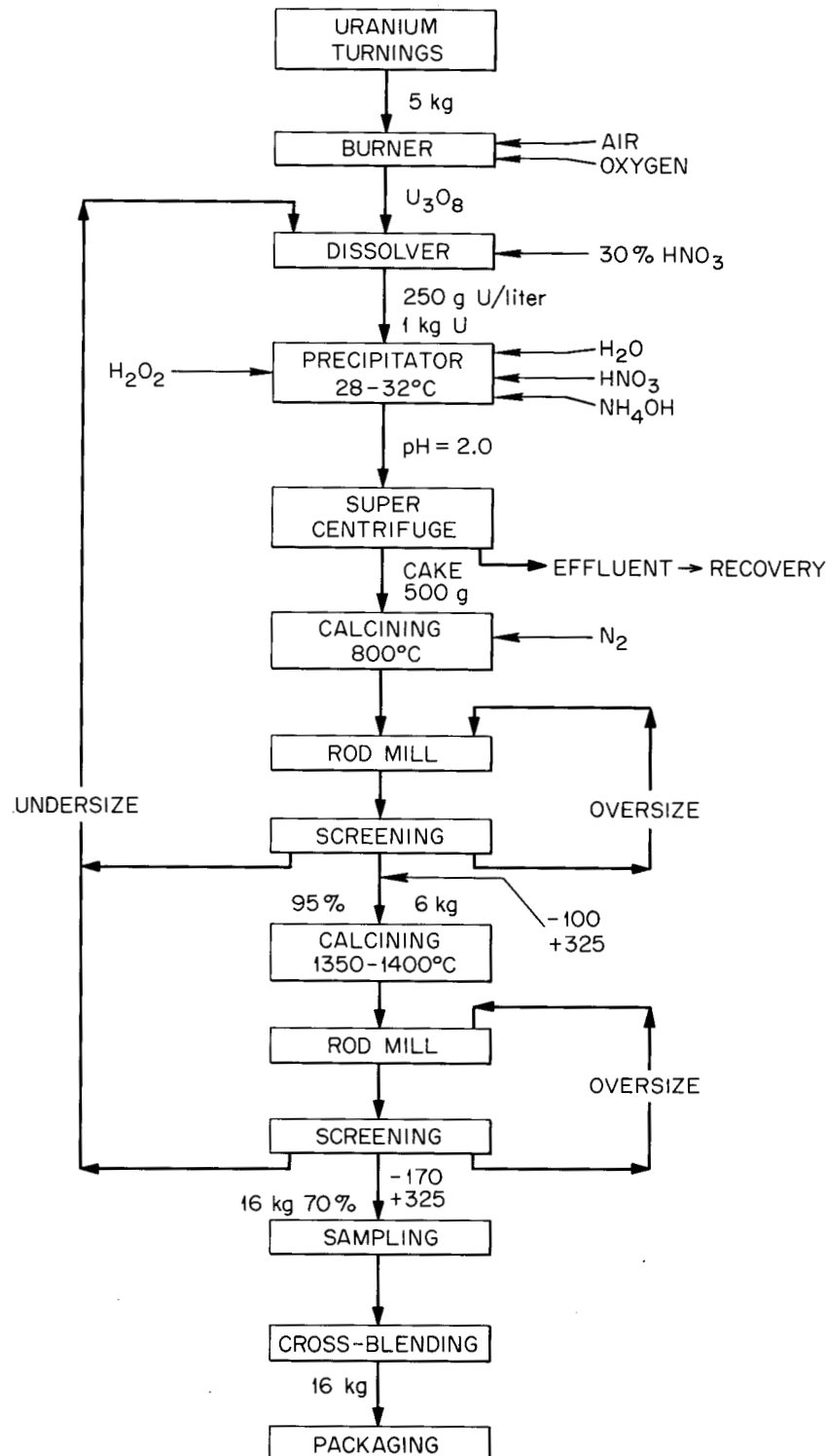
<u>Element</u>	<u>Maximum Impurity Level, ppm</u>	<u>Element</u>	<u>Maximum Impurity Level, ppm</u>	<u>Element</u>	<u>Maximum Impurity Level, ppm</u>
Al	10	Cr	15	Mn	5
B	0.2	Cu	20	Na	5
Ba	10	Fe	100	Ni	20
Be	0.2	K	20	P	<100
Ca	50	F	<10	Si	50
Cd	0.5	Li	1.0	V	2
Co	3	Mg	100		

4. The starting U_3O_8 particle size shall be -170 +325 mesh, as determined in a standard screening test, ASTM B 214-56. This requirement was later modified to permit use of a vibratory screening method rather than a Ro-Tap shaker.

PREPARATION OF U_3O_8

The basic preparation method, diagrammed in Fig. 2, consisted of the precipitation of uranium peroxide from a solution of uranyl nitrate with hydrogen peroxide, followed by calcining and sizing operations. The process was essentially a batch operation utilizing laboratory-type equipment because of the geometry restrictions imposed by nuclear safety and the availability of the equipment from other oxide-production programs. This section details the processing steps that were required to produce the material.

No major problems are encountered in this basic chemical process if the usual precautions with cleanliness are taken. Since it is a batch operation, it is important not to deviate from the procedure for any component part of the process. The yield of product was 85% of the feed material; that is, for every 100 kg of uranium fed into the process, 85 kg of uranium was realized as U_3O_8 .

Fig. 2. U_3O_8 Production Procedure.

The main problem encountered during preparation of the oxide was meeting the $0.05\text{-m}^2/\text{g}$ surface area specification. Calculations show that if all the oxide particles were spherical and of average size ($66\ \mu$), one could expect a surface area of $0.011\ \text{m}^2/\text{g}$. Taking into account the fact that the particles are not spherical and smooth and have a size distribution that includes some fines, one can appreciate the severity of the specification.

Conversion of Metal to U_3O_8 and Dissolution

Uranium machine turnings were burned with oxygen to U_3O_8 in a water-cooled stainless steel burner. The burner was made of type 304L stainless steel 5-in. sched-40 pipe, with an overall length of 40 in. The charge of turnings was limited to 5 kg. After ignition with a match the charge was burned in air until all of the uranium had been converted to oxide (approx 10 min). Burning to U_3O_8 was then completed by the addition of oxygen to the system. Finally, the oxide was removed with a vacuum gulper system.

The U_3O_8 was dissolved in 30% HNO_3 to produce a concentration of approximately 250 g U/liter.

Precipitation

Uranyl nitrate solution containing 1 kg U was transferred to the precipitator and diluted with water to a concentration of approximately 8 wt %. The pH of the solution was adjusted to 2.0 ± 0.1 with nitric acid or ammonium hydroxide. We added 30% H_2O_2 to the precipitator with sufficient ammonium hydroxide to control the pH at 2.0 ± 0.1 . The external cooling water on the precipitator was adjusted to maintain temperature in the range of 28 to 32°C . When the hydrogen peroxide no longer lowered the pH, an additional 500 ml was added and agitation continued for an additional 15 min.

The precipitated uranium peroxide was centrifuged in a Sharples Super Centrifuge and then transferred to platinum boats ($2 \times 4\ 1/2 \times 8$ in.). The peroxide filtrate contains a uranium concentration of 100 to 200 ppm and was economically recoverable, but it was not recycled as feed.

Calcining and Presizing

The boats of uranium peroxide were loaded into a cold electric resistance furnace and calcined for 6 hr at 800°C in an atmosphere of nitrogen. Each boat of uranium peroxide contained approximately 500 g U.

The material was removed from the furnace in the form of agglomerated pieces and presized by dry rod milling and screening to -100 +325 US std mesh (44 to 149 μ). The rod mill was a stainless steel container 5 in. in diameter by 10 in. in length, containing twelve 3/8-in. stainless steel rods. The mills and screens were limited to 1 kg batches of U₃O₈. Mill speed was 275 rpm. Milling time was controlled at 5 min followed by a 10-min sieving cycle in a standard laboratory 8-in. sieve. Syntron vibrating test sieve shakers were used for all sizing operations. This is a change from the specification, where the standard screening test ASTM B 214-56 is specified for testing the final product. During preliminary production comminution of the oxide occurred during this standard screening operation. Subsequently, a Syntron vibrating screen shaker was substituted for the specified Ro-Tap shaker on the basis of the data shown in Table 1. The wet analyses shown in the table, which were performed by washing a 100 g sample of oxide on a 325 mesh screen and collecting the fractions, agree well with the Syntron screen analyses. The degree of comminution caused by the specified standard screen analysis

Table 1. Results of Wet Screen Analyses Followed
by Standard Ro-Tap Analyses

Screening Method	Mesh Size	Part Retained, wt %	
		Blend 1	Blend 2
Syntron analysis	-170 +325	95.6	94.5
	-325	4.4	5.5
Wet analysis	-170 +325	95.84	95.43
	-325	4.16	4.57
ASTM B 214-56 (Ro-Tap analysis)	-170 +325	92.4	92.2
	-325	7.6	7.8

is shown in the lower portion of Table 1. These results were obtained by Ro-Tap analysis of the -170 +325 fraction separated during wet analysis. Approximately 8% additional fines was generated in both cases.

The oversize oxide was recycled through the milling operation and the undersize was dissolved in nitric acid and recycled as feed for the peroxide precipitation step. Approximately 5% fines was generated in the sizing operation for the low-fire step and was recycled.

Sintering and Final Sizing

We loaded 6 kg of low-fired U_3O_8 (sized -100 +325 mesh) into a magnesium oxide crucible 5 1/2 in. in diameter by 9 1/2 in. high. The charge was placed in a Sentry furnace and heated in the ambient atmosphere for 4 hr at 1350°C and then 2 hr at 1400°C. When the oxide had cooled to room temperature, it was milled and sized to -170 +325 mesh (44 to 88 μ) with the same procedure as outlined for the low-fired material. Approximately 30% was lost in the sizing operation from the final product; however, this -325-mesh material was recycled as feed for the peroxide precipitation step.

The furnace used for this operation was No. 4 Sentry 220 v single-phase resistance type with a power capacity of 22.5 kw. A platinum lid covered the crucible in the furnace.

Sampling and Cross Blending

We sampled 16 kg of oxide as a batch after blending in an 8-qt Patterson-Kelley blender. We cross blended lots of nine or ten batches to provide good homogeneity of the oxide by removing a proportionate amount from each batch and reblending in a 4-qt Patterson-Kelley blender. Chemical and physical test data for the more than 300 kg of oxide produced are shown in Table 2 for the blended products and detailed in the appendix for the separate batches. The large variation in size distribution from batch to batch (as seen in the appendix) is attributed to the batch-type operator-dependent operation. We are seeking to improve the uniformity.

Table 2. Chemical and Physical Data of HFIR U_3O_8

	Blend 1	Blend 2	Specification
Total mass, kg	148.1	164.5	
Uranium content, wt %	84.614	84.602	≥ 84.5
Isotopic analysis, wt %			
^{234}U	1.00	1.00	a
^{235}U	93.18	93.16	>93%
^{236}U	0.35	0.33	a
^{238}U	5.47	5.51	a
Surface area (krypton BET determination), m^2/g	0.050	0.047	<0.05
Density (toluene pycnometer), g/cm^3	8.23	8.24	>8.29
UO_2 (x-ray diffraction), %	<1	<1	<1
Fluorine (ppm)	<1	<1	<10
Spectrographic, ppm on U_3O_8 basis			
Al	2	7	10
B	<0.1	<0.1	0.2
Ba	<2	<2	10
Be	<0.01	<0.01	0.2
Ca	<10	<10	50
Cd	<0.1	<0.1	0.5
Co	<1	<1	3
Cr	<2	4	15
Cu	10	8	20
Fe	20	20	100
K	<6	<6	20
Li	<0.2	<0.2	1.0
Mg	3	8	100
Mn	<1	<1	5
Na	<1	<1	5
Ni	5	4	20
P	<100	<100	<100
Si	<10	<10	50
V	<1	<1	2
Stoichiometry (by difference calculation)	$U_3O_{8.015}$	$U_3O_{8.021}$	a
Syntron sieve analysis (100-g sample), %			
+170	0.0	0.2	a
-170 +200	18.9	14.2	a
-200 +230	14.1	14.2	a
-230 +270	30.1	15.6	a
-270 +325	32.5	35.8	a
-325	4.4	5.5	<10%

^aNot specified.

INVESTIGATION OF DIFFERENT GRADES OF OXIDE

During preliminary vendor development of fuel-plate production, the x-ray attenuation inspection technique for fuel homogeneity was found to be sensitive to the grade of oxide employed in the fuel plates.

Fuel plates with commercial oxide consistently exhibited excessive fuel concentrations throughout the core area. First, we assumed that this excess was a result of incorrect rolled core dimensions (i.e., core length and/or width was undersize with an attendant increased core thickness). However, a subsequent examination¹⁶ of the x-ray attenuation data for total uranium contents¹⁷ indicated that the plates contained approximately 6% too much fuel. This result was contradicted by wet chemical analyses of entire plates, which showed that the fuel loadings were within the $\pm 1\%$ specification. Similar previous comparisons of total uranium contents on plates containing Y-12 oxide had agreed within $\pm 0.2\%$. Obviously, there was an x-ray attenuation difference between the oxide used in the ORNL development program and the commercial oxide being used by the vendor. Metallographic examination revealed greater stringering with finer oxide particles in plates made with commercial oxide.

Experimental Investigations

Up to this point the vendor plates under consideration were "process development" plates that were made from commercial depleted oxide. The next step was to determine whether this effect was present in highly enriched reactor-grade plates. Several highly enriched vendor fuel plates were subsequently inspected for total uranium content with both x-ray attenuation techniques and chemical analyses. Once again the plate dissolution studies disagreed with the homogeneity-test results. A comparison of results showed a 3% positive bias in vendor plates containing

¹⁶This examination was performed by B. E. Foster of the Nondestructive Testing Group.

¹⁷B. E. Foster, S. D. Snyder, and R. W. McClung, Continuous Scanning X-Ray Attenuation Techniques for Determining Fuel Inhomogeneities in Dispersion Core Fuel Plates, ORNL-3737 (January 1965).

the commercial oxide. Samples of enriched and depleted commercial oxide were obtained, and the materials were characterized and compared with the Y-12 materials. Throughout the tests identical results were obtained on the depleted and enriched Y-12 oxide; as a result, no distinction is made between these two materials in the characterization studies.

Oxide Microstructure

The morphology and microstructure of Y-12 oxide, depleted commercial oxide, and enriched commercial oxide are shown in Figs. 3 and 4. The Y-12 particles are rounded and glossy with a faceted texture. Microstructurally the particles are sound and, for the most part, exhibited a number of spherical voids, indicative of sintering during processing. Commercial oxide particles, on the other hand, are angular and dull in appearance. Structurally the particles contain a large number of microcracks. The overall impression is that this oxide or portions of it were prepared by the oxidation of initially dense uranium or UO_2 to U_3O_8 and subsequently sized. The basis of this observation lies in the fact that both uranium and UO_2 oxidize with a positive volume change, which leads to the presence of microcracks.

Comminution During Plate Fabrication¹⁸

Comminution of the various oxides during fabrication was studied microradiographically and metallographically. The radiographic technique employed contact radiographs made on extremely fine-grained film that allowed microscopic viewing of details.¹⁹ Representative fields from microradiographs of HFIR fuel plates containing depleted commercial oxide, enriched commercial oxide, and Y-12 oxide (all of initially similar screen analyses) are shown in Fig. 5. As could be predicted from the microstructures of the oxide particles, the depleted commercial oxide

¹⁸B. E. Foster of the Nondestructive Testing Group contributed to this work.

¹⁹R. W. McClung, "Studies in Contact Microradiography," Mater. Res. Std. 4(2), 66-68 (1964).

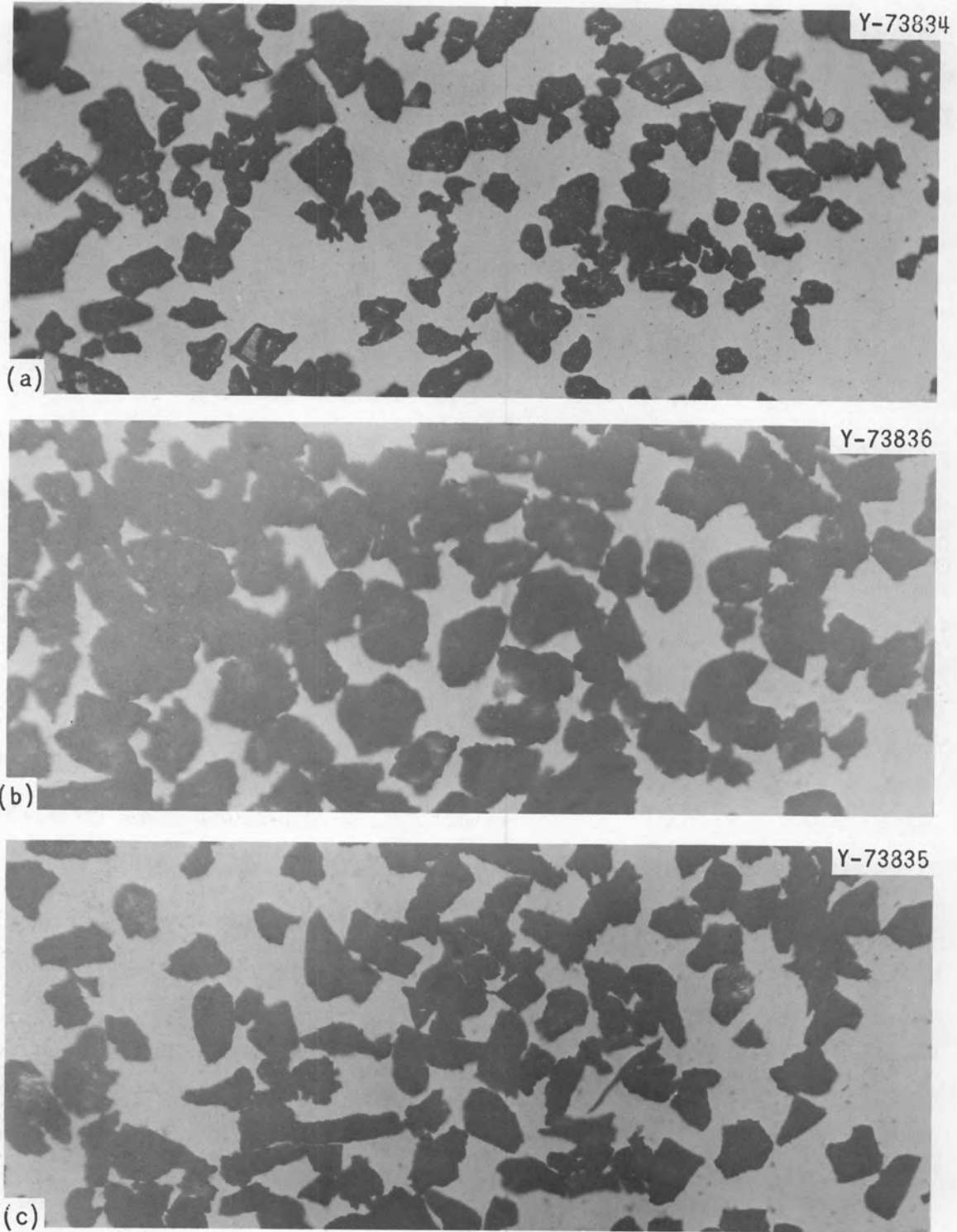


Fig. 3. Morphology of U_3O_8 Particles. 100X. (a) Y-12 material. (b) Commercial depleted material. (c) Commercial enriched material.

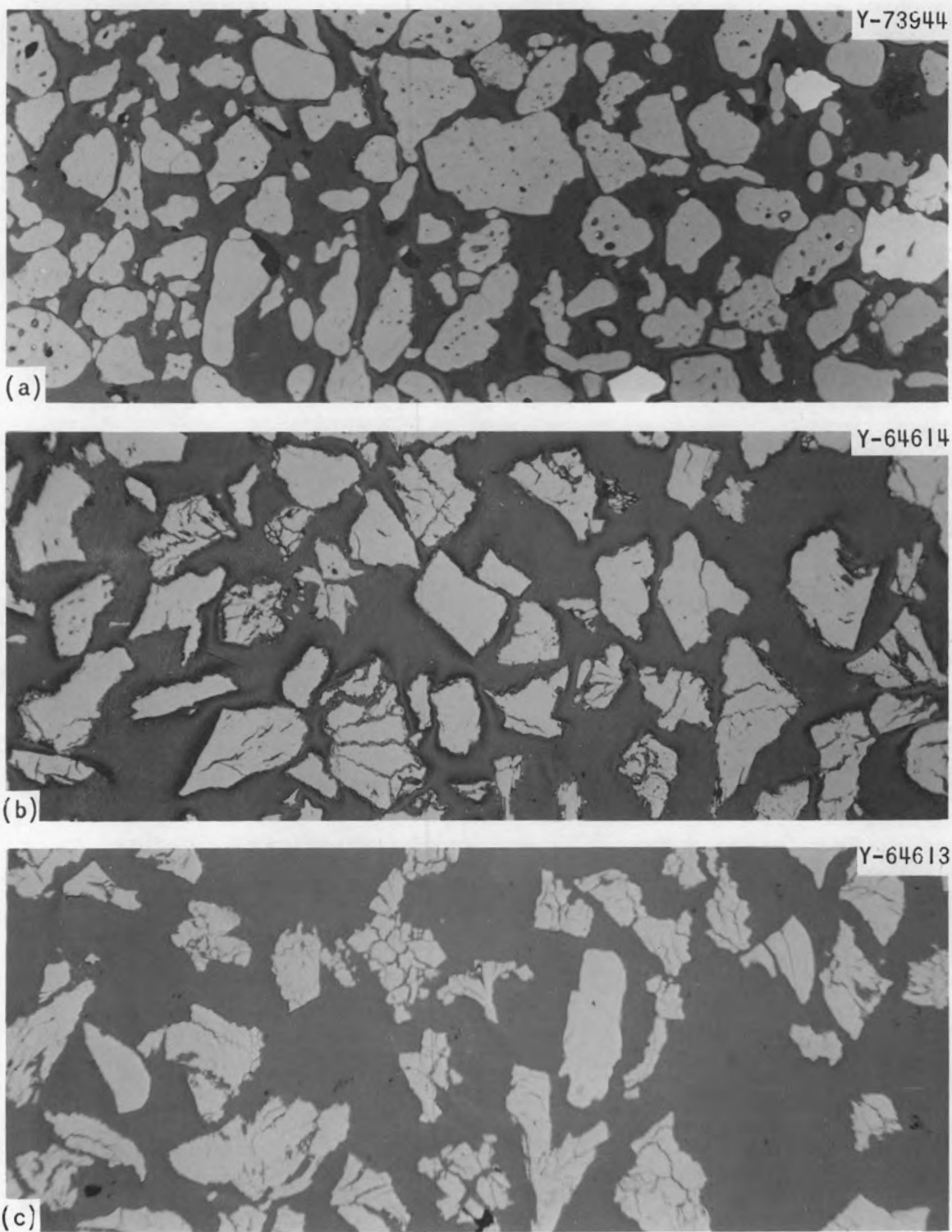


Fig. 4. Microstructure of U_3O_8 Particles. 200X. (a) Y-12 material. (b) Commercial depleted material. (c) Commercial enriched material.

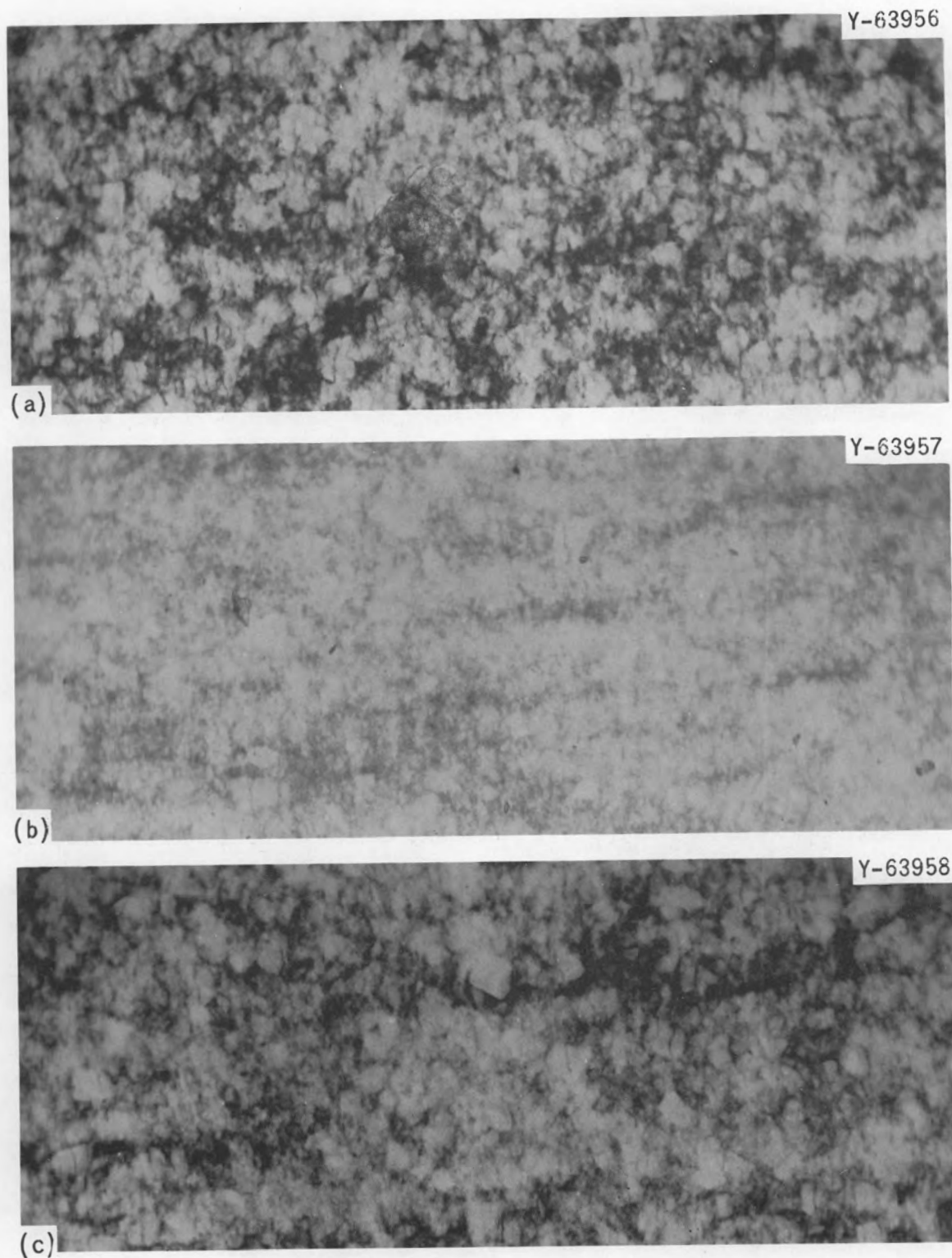


Fig. 5. Microradiographs of the HFIR Fuel Plates Showing Fragmentation Differences. 75X. (a) Y-12 oxide, (b) depleted commercial oxide, and (c) enriched commercial oxide.

exhibited the largest degree of fragmentation and stringering during fabrication. The enriched commercial oxide plate does not show as much fine material and the Y-12 oxide plate shows even less. The metallographic results, shown in Figs. 6-8, were not nearly as vivid. This is because microradiographically we see all the particles in a given plate cross section, whereas metallographically we see only a small portion of the plate cross section. As a result the photomicrographs show less difference in degree of fragmentation. A characterization of fragmentation in such dispersions is reported elsewhere.²⁰

It should be noted that the degree of particle comminution and degree of inspection bias follow similar trends; that is, the smaller the U_3O_8 particle size in the rolled plate, the higher the inspection bias.

X-Ray Studies

Debye-Scherrer powder patterns for Y-12 oxide and enriched commercial oxide (positive prints) obtained in a 114.7-mm-diam camera by exposure to $Cu K\alpha$ radiation for 16 hr are shown in Fig. 9. The spotty appearance of the Debye rings in the Y-12 material indicate that it is rather coarse grained, whereas the smooth rings observed for the vendor oxide indicate a fine grain size. We postulate that the Y-12 oxide is fully sintered and has actually undergone some grain growth during high firing. Careful inspection of the two patterns showed extra lines present at high-angle reflections in the commercial oxide. To negate the possibility of target contamination, we substantiated this result using a very sensitive diffractometer in combination with a scintillation counter and monochromatic radiation. Attempts to identify the extra lines were unsuccessful. We estimate this impurity to be less than 1% of the sample.

²⁰D. O. Hobson and C. F. Leitten, Jr., Characterization of U_3O_8 Dispersion in Aluminum, ORNL-TM-1692 (February 1967).

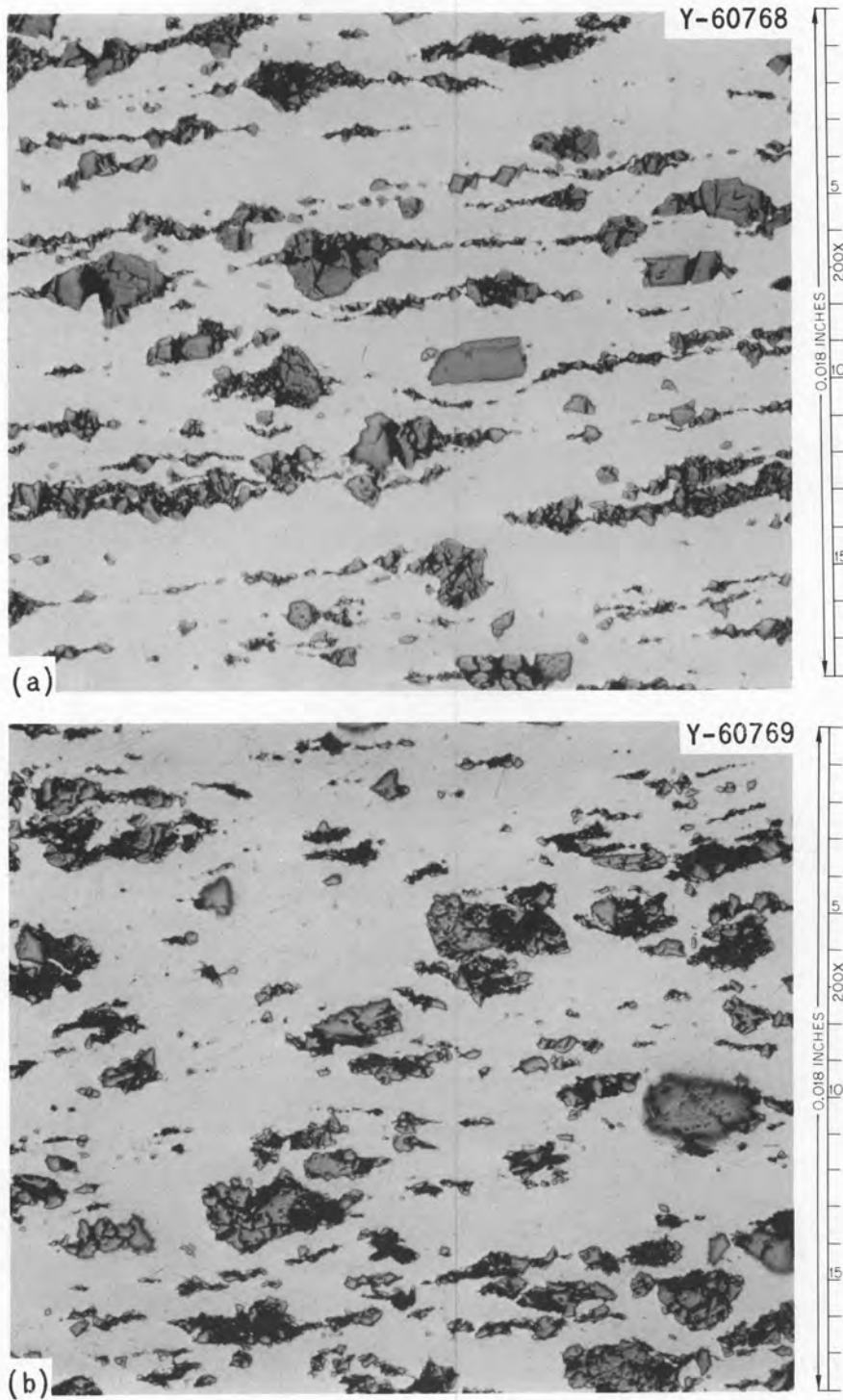


Fig. 6. Microstructure of Vendor-Rolled HFIR Outer Annulus Plate Containing 40.6% Commercial Depleted Oxide. As polished.
(a) Longitudinal section. (b) Transverse section.

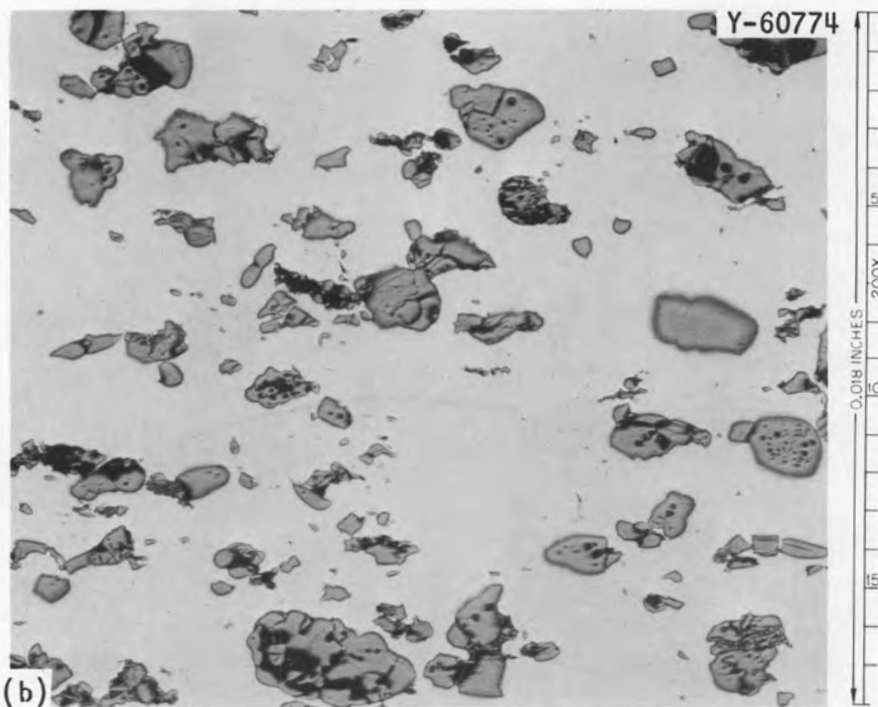
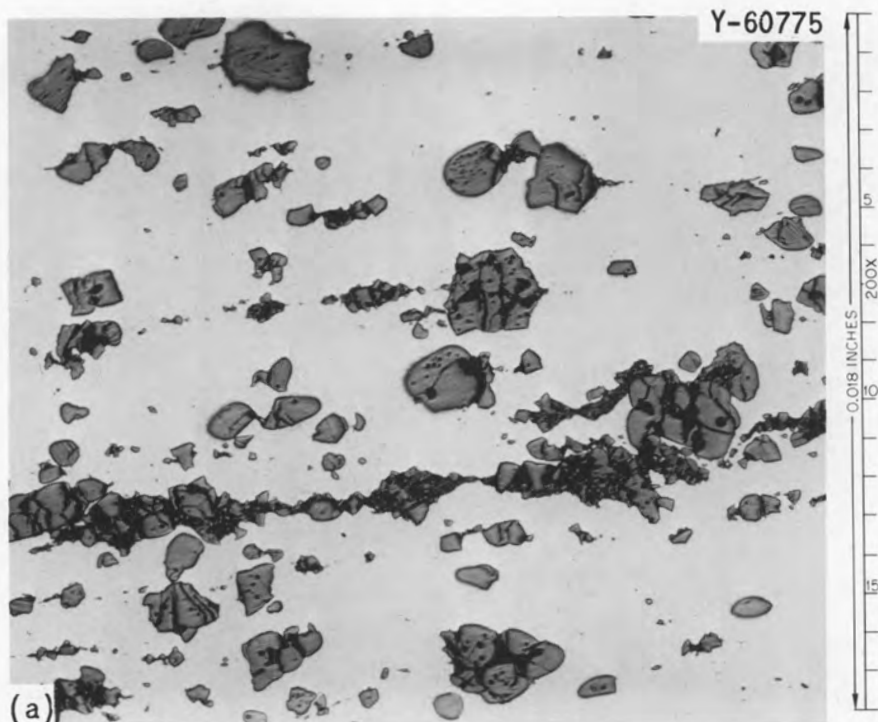


Fig. 8. Microstructure of ORNL-Rolled HFIR Outer Annulus Plate Containing 41.5% Y-12 Depleted Oxide. As polished. (a) Longitudinal section. (b) Transverse section.



Fig. 9. Debye-Scherrer Powder Patterns of (a) Y-12 Oxide and (b) Enriched Commercial Oxide.

Differential Thermal and Thermogravimetric Analyses

Combination DTA-gravimetric tests²¹ were run on the oxides. The DTA compares the temperature of the sample with a neutral sample (Al_2O_3 in this case) while the two are simultaneously heated at a uniform rate. The gravimetric apparatus simultaneously records changes in sample weight of a third sample (in the immediate proximity of the DTA samples) in the same apparatus. The DTA data, when properly interpreted, may show the temperatures at which a phase change, dissociation, reaction, melting or solidification, or recombination of constituents takes place. Furthermore, the presence of one or more materials in the sample may be detected. Figure 10 shows the data obtained on the materials under consideration along with a test on UO_2 to show the sensitivity of the equipment. In all cases the DTA was essentially a straight line; we interpreted this as showing all materials to be essentially pure. Slight thermogravimetric differences between materials were attributed to differences in surface areas between the samples and therefore differences in amounts of adsorbed water.

²¹F. A. Mauer, "Analytical Balance for Recording Rapid Changes in Weight," Rev. Sci. Instr. 25, 598-602 (1954).

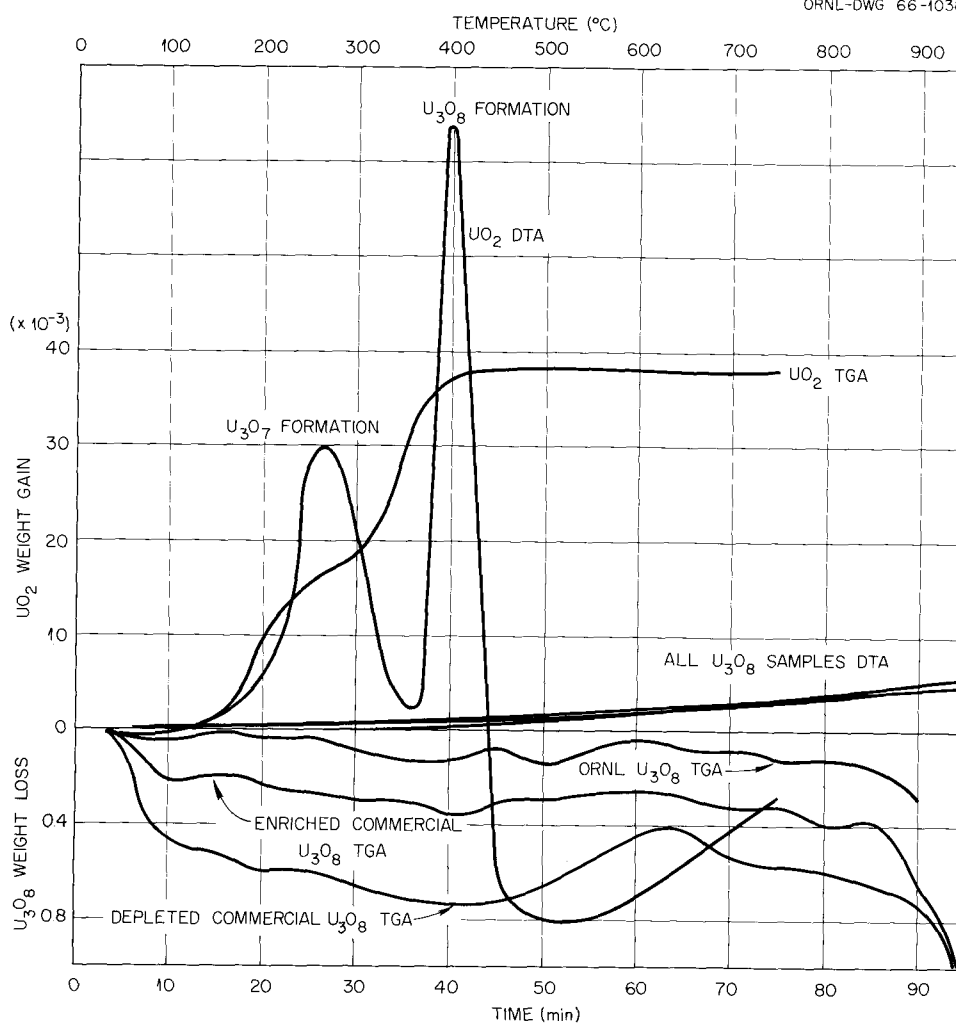


Fig. 10. Combined DTA-TGA Data for U₃O₈ Samples as Compared to UO₂.

Chemical and Surface Area Analysis

Spectrographic analyses for impurity content showed very little differences between the three oxides, with all meeting the specifications as shown in Table 3. The same was true for density (toluene pycnometer) and oxygen-to-uranium ratio. As would be expected from the microstructures, sizable differences were found between static krypton Brunauer-Emmett-Teller (BET) surface-area measurements.

Extensive use has been made of the static nitrogen adsorption method of Brunauer, Emmett, and Teller for determining the surface area

Table 3. Spectrographic Analyses of U_3O_8

Element	Impurity Level of U_3O_8 , ppm		
	Depleted Commercial	Enriched Commercial	ORNL
Aluminum	0.7	14	20
Boron	<2	<2	<4
Barium	3	6	3
Beryllium	<0.01	<0.01	<0.01
Calcium	14	26	14
Cadmium	(a)	(a)	(a)
Cobalt	(a)	(a)	(a)
Chromium	4	8	2
Copper	8	<0.4	25
Iron	15	12	13
Potassium	(a)	(a)	(a)
Fluorine	(a)	(a)	(a)
Lithium	<5	<5	<5
Magnesium	3	5	8
Manganese	0.1	0.5	1
Sodium	<5	<5	<5
Nickel	17	62	4
Phosphorus	<30	<60	<30
Silicon	2	4	2
Vanadium	<2	3	<2

^aNot sought.

of solids.^{22,23} With this method one can determine a relatively large surface area ($>0.5 \text{ m}^2/\text{g}$). However, the nitrogen method is not sufficiently sensitive for the measurement of surface areas smaller than $0.5 \text{ m}^2/\text{g}$. The major limiting factor is the large correction necessary for unadsorbed nitrogen gas, which stems from the high saturation pressure of nitrogen (approx 1 atm at -195.8°C). This limitation in turn causes a deviation from the ideal gas law. The absorption of krypton vapor is well suited

²²S. Brunauer, P. H. Emmett, and E. Teller, "Adsorption of Gas in Multimolecular Layers," J. Am. Chem. Soc. 60, 309 (1938).

²³R. L. Walker, "Surface Area of Powdered Solid, Nitrogen Adsorption Method," Method Nos. 1 102 and 9 00602 (1-15-58) ORNL Master Analytical Manual, TTD 7015, Supplement 1 (November 1959).

for surface-area measurement by the BET method, and its saturation pressure is only about 2 mm at -195.8°C . Krypton will deviate from ideal gas behavior only by an undetectable amount because of the relatively small volume of unadsorbed gas. Therefore, if krypton is used instead of nitrogen, specific surface areas in the range from 0.01 to $0.5 \text{ m}^2/\text{g}$ can be measured.²⁴

Theoretically, a monomolecular layer of krypton is adsorbed on the surface of a solid at a pressure of 0.1 to 1 mm when the temperature of the solid is -195.8°C , which is the temperature of liquid nitrogen at a pressure of 760 mm. Based on this theory, calculations²⁵ show that a single molecule of krypton covers an area of $19.5 \pm 0.04 \text{ \AA}^2$ of a solid whose temperature is -195.8°C . From the theory of monomolecular adsorption, the knowledge of the area covered by a single molecule of krypton, and Avogadro's number, the area of a solid covered by 1 cm^3 of krypton has been found to be 4.05 m^2 . With this value one can calculate the surface area of a solid from the experimentally determined volume of krypton gas that is adsorbed on a known weight of the solid under the conditions for monomolecular adsorption. The volume of krypton, in cubic centimeters at standard temperature and pressure, that forms a monomolecular layer on the surface of the solid can be determined from the slope and the intercept of a BET plot, which is a rectilinear plot of $X/V_a(1 - X)$ vs X , where V_a is the volume of krypton adsorbed at pressure P and at a temperature at which the vapor pressure of krypton is P/X .

The BET static surface areas found for the various grades of oxide follow.

<u>Type Material</u>	<u>Surface Area, m^2/g</u>
Depleted vendor oxide	0.13
Enriched vendor oxide	0.08
Y-12 oxide	0.05
Specified	0.05

²⁴J. L. Botts, "Surface Area of Solids, Krypton Adsorption Method," Method Nos. 1 105 and 9 00605 (12-28-61) ORNL Master Analytical Manual, TID-7015, Supplement 5 (September 1963).

²⁵R. A. Beebe, J. B. Beckwith, and J. M. Honig, "The Determination of Small Surface Areas by Krypton Adsorption at Low Temperatures," J. Am. Chem. Soc. 67, 1554 (1945).

These results are in direct agreement with the observed particle microstructures, which show cracked irregular particles for the commercial oxide and not for sintered Y-12 oxide.

X-Ray Attenuation Differences

In the initial calibration of the x-ray attenuation homogeneity inspection scanner it was recognized that changes in fissile material particle size could necessitate recalibration of the instrument. An analysis of the effect of oxide particle size in a fabricated plate on x-ray attenuation resulted in the following explanation of the inspection bias. Consider a U_3O_8 -aluminum dispersion plate of constant thickness T in which the thickness of fissile particles at any thickness position is x . If we treat the matrix as a void (which we can do in this case because the absorption coefficient of aluminum is very much smaller than that of uranium), the ratio of transmitted to incident radiation is given by Lambert's law: $I/I_0 = e^{-\mu x}$. If we are inspecting a finite volume of a fuel plate (5/64-in.-diam beam), we are dealing with average values; therefore the equation can be written:

$$\langle I/I_0 \rangle = \langle e^{-\mu x} \rangle$$

or

$$\langle I/I_0 \rangle = e^{-\mu \langle x \rangle} \langle e^{-\mu(x - \langle x \rangle)} \rangle ,$$

where we can expand

$$\begin{aligned} \langle e^{-\mu(x - \langle x \rangle)} \rangle &= \langle 1 - \mu(x - \langle x \rangle) + \frac{\mu^2(x - \langle x \rangle)^2}{2!} - \dots \rangle \\ &= 1 + \mu^2(\langle x^2 \rangle - \langle x \rangle^2)/2 , \end{aligned}$$

ignoring terms in x^3 and higher powers, since they will be quite small.

Then

$$\langle I/I_0 \rangle = e^{-\mu \langle x \rangle} [1 + \mu^2(\langle x^2 \rangle - \langle x \rangle^2)/2] ,$$

where the term $(\langle x^2 \rangle - \langle x \rangle^2)$ is a measure of particle size and/or distribution. For example, consider the two systems of identical uranium content shown in Fig. 11. In system 1 the uranium is distributed on an atomic scale and the $\langle x \rangle$ is uniform across the plate. In this case $\langle x \rangle$ and x are equal at all points, so $\langle I/I_0 \rangle = e^{-\mu \langle x \rangle}$. In system 2, x varies from zero to a maximum, so the difference between $\langle x^2 \rangle$ and $\langle x \rangle^2$ will be a maximum. This same situation is shown qualitatively in Fig. 12 where $\langle e^{-\mu x} \rangle > e^{-\mu \langle x \rangle}$. The difference between the terms will, of course, be larger for large variations in x . Since the scanner was calibrated according to the equation $\langle I/I_0 \rangle = e^{-\mu \langle x \rangle}$, changes in oxide particle size affect the calibration of the instrument. In the case of the commercial oxide, which fragmented more than the Y-12 oxide, the result was an apparent excessive fuel concentration.

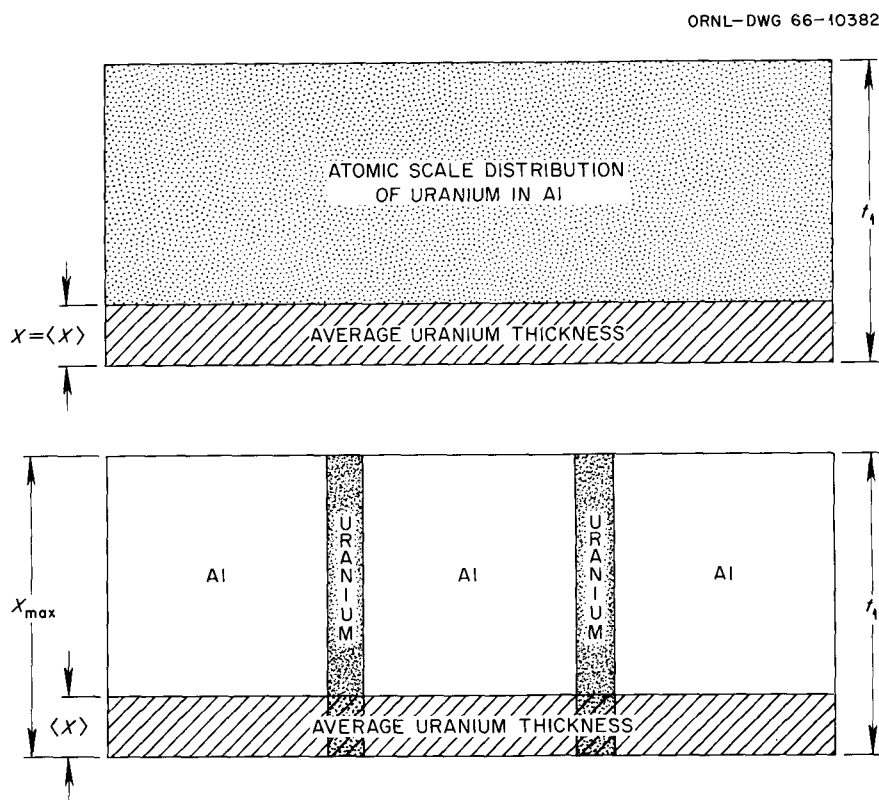


Fig. 11. Schematic Illustration of Two Systems of Identical Uranium Content and Different Distribution. (a) Atomic scale distribution of uranium, in which the thickness of uranium at any position is equal to the average value of the uranium thickness $x = \langle x \rangle$. (b) Segregated uranium distribution, where $x > \langle x \rangle$.

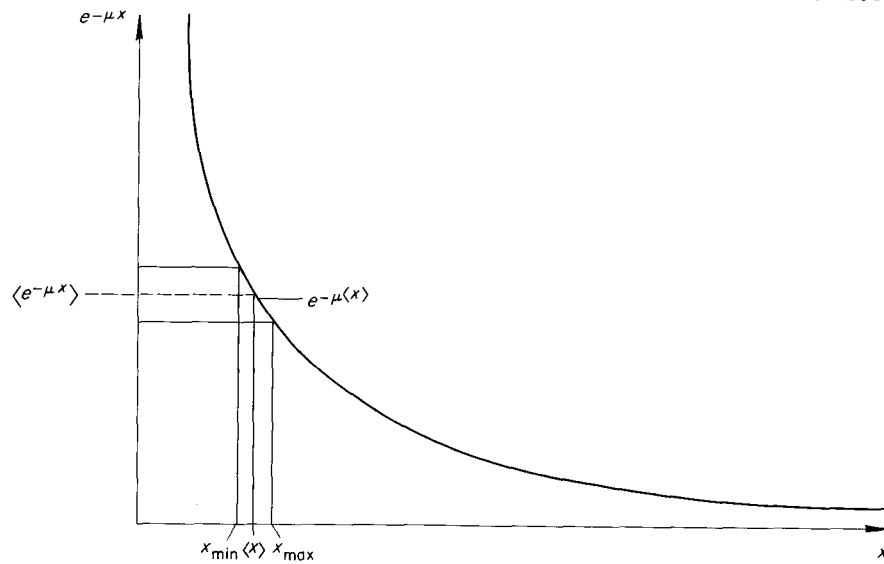


Fig. 12. Graphical Illustration of the Difference Between $e^{-\mu \langle x \rangle}$ and $\langle e^{-\mu x} \rangle$.

CONCLUSIONS

A process developed by the Y-12 facility was used to produce oxide for the first vendor-made HFIR fuel elements. The process was repetitive over many production batches. The yield of oxide produced was 85% of the feed material; that is, for every 100 kg of uranium fed into the process, 85 kg of uranium was realized as final product.

We compared a commercial oxide with Y-12 oxide and found the Y-12 material to be superior for HFIR application. Of particular concern was the propensity of this commercial oxide toward fragmentation and stringering during fuel-plate fabrication. Characterization studies showed this property to be directly related to the microstructure and morphology of the original particles. The Y-12 particles are rounded and glossy, with a faceted texture. Microstructurally, the particles are sound and, for the most part, exhibit a number of spherical voids, indicative of sintering during processing. The commercial oxide particles, on the other hand, are angular and dull in appearance. Structurally the particles contain a large number of microcracks. An evaluation of the oxide characterization data showed that surface area

was a good criterion for evaluation of oxide integrity, since there were obvious correlations between this property and production method, microstructure, and comminution during fabrication. We specified the static krypton BET surface area determination method because of our experience with its precision and accuracy.

ACKNOWLEDGMENTS

Acknowledgment is due G. M. Adamson, Jr. for program administration and coordination. Special acknowledgment is due B. E. Foster for his suggestions and assistance during this investigation and Bernard Borie for his explanation of the x-ray attenuation dependence on U_3O_8 particle size. Also to the Analytical Chemistry Division, the X-Ray Diffraction Group, the Ceramics Laboratory, and the Nondestructive Testing Group of the Metals and Ceramics Division we express appreciation for their contributions. We express thanks to the Metallography Group, the Reports Office, and Sigfred Peterson for contributions to the preparation of this report.

APPENDIX

Analytical Data on the Individual Batches of U_3O_8



Batches Constituting Blend 1

	Batch								
	169346	169349	169407	169410	169412	169414	169416	169422	169355
Grams U/g	84.6522	84.659	84.623	84.628	84.669	84.660	84.621	84.655	84.668
²³⁴ U	0.97	0.99	0.97	1.00	1.00	1.01	0.97	1.00	1.00
²³⁵ U	93.20	93.14	93.20	93.14	93.19	93.09	93.18	93.13	93.16
²³⁶ U	0.31	0.32	0.30	0.32	0.34	0.39	0.36	0.35	0.36
²³⁸ U	5.52	5.55	5.53	5.54	5.47	5.51	5.49	5.52	5.48
Aluminum	<1	2	3	6	1	3	4	3	1
Boron	<0.1	<0.1	<0.1	<0.1	<0.1	<0.1	<0.1	<0.1	<0.1
Barium	<2	<2	<2	<2	<2	<2	<2	<2	<2
Beryllium	<0.01	<0.01	<0.01	<0.01	<0.01	<0.01	<0.01	<0.01	<0.01
Calcium	<10	<10	<10	<10	<10	<10	<10	<10	<10
Cadmium	<0.1	<0.1	<0.1	<0.1	<0.1	<0.1	<0.1	<0.1	<0.1
Cobalt	<1	<1	<1	<1	<1	<1	<1	<1	<1
Chromium	2	<2	<2	6	<2	7	4	5	<2
Nickel	4	4	3	8	4	4	2	6	4
Iron	15	20	20	50	30	60	50	75	15
Copper	6	8	6	10	6	8	5	20	8
Potassium	<6	<6	<6	<6	<6	<6	<6	<6	<6
Lithium	<0.2	<0.2	<0.2	<0.2	<0.2	<0.2	<0.2	<0.2	<0.2
Magnesium	<2	5	15	15	8	30	3	10	6
Manganese	<1	<1	<1	<1	<1	<1	<1	<1	<1
Sodium	1	<1	<1	2	<1	<1	<1	2	<1
Phosphorus	<100	<100	<100	<100	<100	<100	<100	<100	<100
Silicon	<10	<10	12	12	<10	10	<10	<10	10
Vanadium	<1	<1	<1	<1	<1	<1	<1	<1	<1
Fluorine	<1	1.4	<1	<1	<1	<1	<1	<1	<1
UO ₂	<1%	<1%	<1%	<1%	<1%	<1%	<1%	<1%	<1%
Density	8.23	8.23	8.25	8.23	8.24	8.25	8.25	8.26	8.26
Surface area	0.049	0.049	0.048	0.051	0.049	0.052	0.051	0.055	0.056
Kilogram U ₃ O ₈	16.3	16.2	16.2	16.6	16.6	16.6	16.5	16.5	16.6
<u>Screen Size</u>									
+170	0	0	0.2	0	0.5	0	0.2	0.2	0
-170 +200	21.4	17.3	15.7	9.0	25.5	18.5	18.4	18.8	13.0
-200 +230	20.8	19.3	24.0	20.4	18.6	18.1	21.8	19.7	21.9
-230 +270	14.6	15.7	12.5	18.0	13.7	15.6	13.6	17.5	14.4
-270 +325	39.1	41.6	41.1	47.4	35.8	42.9	39.8	38.6	45.6
-325	4.1	6.1	6.5	5.2	5.9	4.9	6.3	5.2	5.1

Batches Constituting Blend 2

	Batch									
	169348	169405	169408	169411	169413	169415	169350	169357	169359	169360
Grams U/g	84.672	84.682	84.657	84.703	84.637	84.698	84.656	84.606	84.653	84.676
²³⁴ U	0.96	0.95	0.99	0.98	1.00	1.04	0.99	0.94	1.01	1.01
²³⁵ U	93.19	93.16	93.18	93.18	93.12	93.09	93.15	93.17	93.12	93.16
²³⁶ U	0.31	0.27	0.30	0.32	0.35	0.36	0.34	0.33	0.36	0.31
²³⁸ U	5.54	5.62	5.53	5.52	5.53	5.51	5.52	5.56	5.51	5.52
Aluminum	2	5	3	5	2	3	4	1	1	1
Boron	<0.1	<0.1	<0.1	<0.1	0.1	0.1	<0.1	<0.1	<0.1	<0.1
Barium	<2	<2	<2	<2	<2	<2	<2	<2	<2	<2
Beryllium	<0.01	<0.01	<0.01	<0.01	<0.01	<0.01	<0.01	<0.01	<0.01	<0.01
Calcium	<10	<10	<10	<10	<10	<10	<10	<10	<10	<10
Cadmium	<0.1	<0.1	<0.1	<0.1	0.1	<0.1	<0.1	<0.1	<0.1	<0.1
Cobalt	<1	<1	<1	<1	<1	<1	<1	<1	<1	<1
Chromium	<2	4	<2	6	4	4	5	<2	2	2
Nickel	5	8	3	6	4	6	6	5	2	2
Iron	15	30	30	55	80	60	75	25	40	45
Copper	8	7	6	10	25	6	15	10	4	4
Potassium	<6	<6	<6	<6	<6	<6	<6	<6	<6	<6
Lithium	<0.2	<0.2	0.3	<0.2	<0.2	<0.2	<0.2	<0.2	<0.2	<0.2
Magnesium	8	10	7	6	12	30	10	8	4	4
Manganese	<1	1	<1	<1	<1	2	<1	<1	<1	<1
Sodium	<1	<1	<1	<1	<1	<1	<1	<1	<1	<1
Phosphorus	<100	<100	<100	<100	<100	<100	<100	<100	<100	<100
Silicon	10	15	<10	10	<10	<10	<10	15	<10	12
Vanadium	<1	<1	<1	<1	<1	<1	<1	<1	<1	<1
Fluorine	<1	<1	<1	<1	<1	<1	<1	<1	<1	<1
UO ₂	<1%	<1%	<1%	<1%	<1%	<1%	<1%	<1%	<1%	<1%
Density	8.26	8.27	8.22	8.22	8.26	8.23	8.27	8.27	8.26	8.26
Surface area	0.048	0.049	0.049	0.045	0.052	0.054	0.057	0.052	0.048	0.054
Kilogram U ₃ O ₈	16.3	16.3	16.2	16.5	16.5	16.5	16.6	16.6	16.3	16.7
<u>Screen Size</u>										
+170	0	0.2	0	0	0.2	0	0	0	0.1	0.1
-170 +200	20.0	24.8	18.3	10.3	17.7	16.3	12.3	12.6	21.0	18.8
-200 +230	19.3	17.0	19.3	22.2	20.6	20.5	19.6	15.7	11.8	14.7
-230 +270	14.9	14.6	13.9	15.3	14.8	13.5	16.2	27.8	29.2	28.0
-270 +325	41.4	38.0	40.6	43.8	41.3	43.7	45.6	39.0	33.8	34.3
-325	4.4	5.4	7.9	8.4	5.4	6.0	6.3	4.9	4.1	4.1

ORNL-4052
UC-25 - Metals, Ceramics, and Materials

INTERNAL DISTRIBUTION

1-3.	Central Research Library	33.	B. E. Foster
4-5.	ORNL - Y-12 Technical Library	34.	J. H. Frye, Jr.
	Document Reference Section	35-37.	M. R. Hill
6-15.	Laboratory Records	38.	D. O. Hobson
16.	Laboratory Records, ORNL R.C.	39.	R. W. Knight
17.	ORNL Patent Office	40.	C. E. Larson
18.	G. M. Adamson, Jr.	41.	H. G. MacPherson
19-23.	J. R. Barkman (Y-12)	42.	M. M. Martin
24.	R. J. Beaver	43.	W. R. Martin
25.	A. L. Boch	44.	H. F. McDuffie
26.	G. E. Boyd	45.	S. Peterson
27.	G. L. Copeland	46.	S. D. Snyder
28.	J. A. Cox	47.	J. T. Venard
29.	F. L. Culler	48-52.	W. J. Werner
30.	J. E. Cunningham	53.	A. M. Weinberg
31.	J. H. Erwin	54.	M. B. Bever (consultant)
32.	D. E. Ferguson	55.	A. R. Kaufmann (consultant)
		56.	J. A. Krumhansl (consultant)

EXTERNAL DISTRIBUTION

57. J. Binns, Metals and Controls Corporation, Attleboro, Mass.

58. D. F. Cope, RDT, OSR, AEC, Oak Ridge National Laboratory

59. D. R. deBoisblanc, Phillips Petroleum Corporation, AED

60. J. L. Gregg, Bard Hall, Cornell University

61. Ray Jones, AEC, Washington

62. E. A. Kintner, AEC, Washington

63. W. J. Larkin, AEC, Oak Ridge Operations

64. P. W. McDaniel, AEC, Washington

65. D. D. Rausch, AEC, Washington

66. H. M. Roth, AEC, Oak Ridge Operations

67. J. M. Simmons, AEC, Washington

68. E. E. Stansbury, University of Tennessee

69. J. A. Swartout, Union Carbide

70. W. W. Ward, AEC, Washington

71. Research and Development Division, AEC, Oak Ridge Operations

72-343. Given distribution as shown in TID-4500 under Metals, Ceramics, and Materials category (25 copies - CFSTI)